PCCP

Substitution effect on the nonradiative decay and trans → cis photoisomerization route: a guideline to develop efficient cinnamate based sunscreens

Journal:	*Physical Chemistry Chemical Physics*
Manuscript ID	CP-ART-08-2020-004402.R1
Article Type:	Paper
Date Submitted by the Author:	30-Oct-2020

Complete List of Authors:	Kinoshita, Shin-nosuke; Hiroshima university Harabuchi, Yu; Hokkaido University Inokuchi, Yoshiya; Hiroshima university Maeda, Satoshi; Hokkaido University Ehara, Masahiro; Institute for Molecular Science Yamazaki, Kaoru; Riken Ebata, Takayuki; National Chiao Tung Universitry

ARTICLE

Substitution effect on the nonradiative decay and *trans* → *cis* photoisomerization route: a guideline to develop efficient cinnamate based sunscreens

Received 00th January 20xx,
Accepted 00th January 20xx

DOI: 10.1039/x0xx00000x

Shin-nosuke Kinoshita,[a] Yu Harabuchi,[b, c] Yoshiya Inokuchi,[a] Satoshi Maeda,[b, c] Masahiro Ehara,[d, e] Kaoru Yamazaki,*[f, g] and Takayuki Ebata *[a, h]

Cinnamate derivatives are very useful as a UV protector in nature and a sunscreen reagent in our daily life. They convert harmful UV energy to thermal one through the effective nonradiative decay (NRD) including *trans* → *cis* photoisomerization. However, the mechanism is not simple because different photoisomeirzation routes have been observed for the different substituted cinnamates. Here, we theoretically examined the substitution effects at the phenyl ring of methylcinnamate (MC), the non-substituted cinnamate, on the electronic structure and the NRD route involving the *trans* → *cis* isomerization based on time-dependent density functional theory (TD-DFT). The systematic reaction pathway search using the single-component artificial force induced reaction (SC-AFIR) method shows that the very efficient photoisomerization route of MC is essentially described as "$^1\pi\pi^*$ (*trans*) → $^1n\pi^*$ → T_1 ($^3\pi\pi^*$) → S_0 (*trans* or *cis*)". We found that for the efficient $^1\pi\pi^*$ (*trans*) → $^1n\pi^*$ internal conversion (IC), MC should have the substituent at the appropriate position of the phenyl ring to stabilize the highest occupied π orbital. The substitution at *para* position of MC slightly lowers the $^1\pi\pi^*$ state energy and photoisomerization undergoes *via* slightly less efficient "$^1\pi\pi^*$ (*trans*) → $^3n\pi^*$ → T_1 ($^3\pi\pi^*$) → S_0 (*trans* or *cis*)" pathway. The substitution at *meta* or *ortho* position of MC significantly lowers the $^1\pi\pi^*$ state energy so that the energy barrier of IC ($^1\pi\pi^*$ → $^1n\pi^*$) becomes very high. This substitution leads to the much longer $^1\pi\pi^*$ state lifetime than MC and *para*-substituted MC, and a change of the dominant photoisomerization route to "$^1\pi\pi^*$ (*trans*) → C=C bond twisting on $^1\pi\pi^*$ → S_0 (*trans* or *cis*)". As a whole, the "$^1\pi\pi^*$ → $^1n\pi^*$" IC observed in MC is the most important initial step for the rapid change of the UV energy to thermal one. We also found that the stabilization of the π orbital (i) minimizes the energy gap between $^1\pi\pi^*$ and $^1n\pi^*$ at the $^1\pi\pi^*$ minimum, and (ii) makes the 0-0 level of $^1\pi\pi^*$ higher than $^1n\pi^*$ as observed in MC. These MC-like relationships between the $^1\pi\pi^*$ and $^1n\pi^*$ energies should be ideal to maximize the "$^1\pi\pi^*$ → $^1n\pi^*$" IC rate constant according to Marcus theory.

1. Introduction

Cinnamic acids and cinnamates, that have unsaturated carboxylic or ester group on their phenyl group, widely exist in nature such as lignin in plants[1-4] and in bacteria as a chromophore.[5,6] In our daily life, cinnamates gain attention as the potential protective role against oxidative damage disease[7] and as UV protection reagents for sunscreen cosmetics, such as known as octinoxate or octyl methoxycinnamate.[8,9] Cinnamates take a stable *trans* (*E*) form in the electronic ground state (S_0). Upon the UV absorption, they are mostly excited to the bright $^1\pi\pi^*$ state and rapidly relax *via* several nonradiative decay (NRD) process, and finally return to the *trans* (*E*) form or isomerize to *cis* (*Z*) form.[10-14]

Here, the rapid NRD from the $^1\pi\pi^*$ state and an efficient conversion of the UV energy to thermal one (vibrational energy) without producing harmful biproducts may be highly desired for the good sunscreen reagent. The *trans* → *cis* and *cis* → *trans* photoisomerization is the reversible process.[12, 14] Shindo *et al*. examined the quantum yield (ϕ) for each process for ethylcinnamate (EC) in ethanol solution.[14] They obtained ϕ (*trans* → *cis*) is 0.26 and ϕ (*cis* → *trans*) is 0.29, and suggested that the half of the photoexcited species directly deactivates to S_0 of the same isomeric form, and the other half isomerizes *via* the singlet and/or triplet states. This is in accordance with the very recent work of Krokidi *et al*. who observed two competing deactivation routes in cyclohexane solution.[15] As to the photophysics of the *cis*-isomer, recently Zhao *et*

[a] Department of Chemistry, Graduate School of Science, Hiroshima University, Higashi-Hiroshima 739-8526, Japan. E-mail: tebata@hiroshima-u.ac.jp
[b] Department of Chemistry, Faculty of Science, Hokkaido University, Sapporo 060-0810, Japan
[c] Institute for Chemical Reaction Design and Discovery (WPI-ICReDD), Hokkaido University, Sapporo 001-0021, Japan.
[d] SOKENDAI, the Graduate University for Advanced Studies, Myodaiji, Okazaki 444-8585, Japan
[e] Institute for Molecular Science and Research Center for Computational Science,38 , Myodaiji, Okazaki 444-8585, Japan.
[f] Institute for Materials Research, Tohoku University, Katahira 2-1-1, Aoba-ku,Sendai, 980-8577, Japan. E-mail: kaoru.yamazaki@imr.tohoku.ac.jp
[g] Present address： Attosecond Science Research Team, RIKEN Center for Advanced Photonics, 2-1 Hirosawa, Wako, Saitama, 351-0198, Japan. E-mail: kaoru.yamazaki@riken.jp
[h] Present address ： Department of Applied Chemistry, National Chiao Tung University, Hsinchu 30010, Taiwan. E-mail: tebata@nctu.edu.tw
Electronic Supplementary Information (ESI) available: [details of any supplementary information available should be included here]. See DOI: 10.1039/x0xx00000x

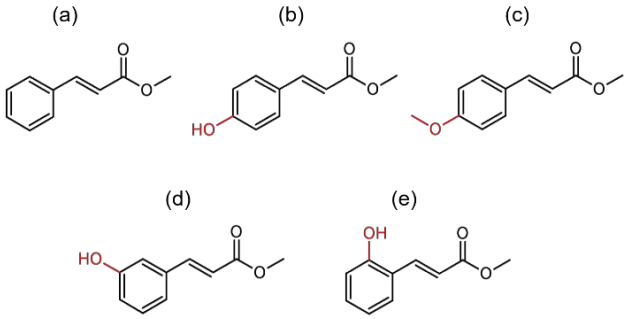

Chart 1. Chemical structure of (a) methylcinnamate (MC), (b) *para*-hydroxy MC (*p*-HMC), (c) *para*-methoxy MC (*p*-MMC), (d) *meta*-HMC (*m*-HMC) and (e) *ortho*-HMC (*o*-HMC).

al. reported that the lifetime of the $^1\pi\pi^*$ state of the *cis*-isomer is shorter than that of *trans* in methyl sinapate, and proposed that two NRD routes, adiabatic and nonadiabatic relaxations, compete in the *cis*-isomer, making the short lifetime of the *cis*-isomer.[3]

The investigation of the electronic states, their lifetime and photophysics involving the photoisomerization have been carried out experimentally using UV and IR spectroscopy, and time-resolved spectroscopy, as well as by theoretical calculations to quest these issues.[1-54]

The $^1\pi\pi^*$ state lifetime of the cinnamates and cinnamic acids in the gas-phase is in the range from a few picoseconds to a few tens of nanoseconds, which is quite different depending on the substituents on phenyl group.[16-23] For example, the lifetime of $^1\pi\pi^*$ of methylcinnamate (MC) is first reported to be less than 10 ps by picosecond pump-probe spectroscopy by Kinoshita *et al.*[21] and recently obtained to be 4.5 ps by femtosecond pump-probe spectroscopy.[15] A substitution of the OH group at the *para*-position of MC leads little change on the $^1\pi\pi^*$ lifetime, while the substitution at *ortho*- or *meta*-position elongates the lifetime by three orders of magnitude.[17,19] On the other hand, the substitution effect at the ester part on the $^1\pi\pi^*$ lifetime is rather small. For example, the reported $^1\pi\pi^*$ lifetime of *para*-methoxy MC (*p*-MMC), *para*-methoxy EC, and octyl methoxycinnamate is 280 ps, 70 ps and 40 ps, respectively.[17,18,22] In addition, recent work on sinapate ester indicates that the efficiency of photoprotection is independent of *trans* (*E*) or *cis* (*Z*) isomer.[24,25] Thus, it is considered that for the development of effective sunscreen reagent, a modification of the phenyl group is more efficient.

Form our previous studies, we pointed out three important issues to investigated the NRD involving the isomerization in the gas phase. First is the detection and assignment of the transient electronic state generated during the NRD process. The transient electronic state was first observed for *para*-substituted cinnamates by using nanosecond pump-probe spectroscopy with the probe (ionization) laser fixed at 193 nm.[26] Later, the transient electronic state was assigned to the T_1 ($^3\pi\pi^*$) state for MC, *p*-hydroxy MC (*p*-HMC) and *p*-MMC shown in Chart 1 (a)-(c) by determining its energy using tunable deep UV (DUV) laser and by quantum chemical calculation.[18,19,21]

Second is the detection of the $^1n\pi^*$ state. Although the internal conversion (IC) from $^1\pi\pi^*$ to $^1n\pi^*$ is thought to be the key NRD process, the $^1n\pi^*$ state was hardly detected due to a very small oscillator strength from S_0 and an interference by the nearby $^1\pi\pi^*$ absorption. However, the $^1n\pi^*$ state has been recently observed for MC by our group.[21] The state is located at 660 cm^{-1} (0.082 eV) below $^1\pi\pi^*$. It was also found that the substitution to the phenyl ring reverses the order of their energies.

Third is the substitution position dependence of the NRD / photoisomerization route. We reported that in the structural isomers of HMC (*p*-, *m*-, *o*-HMC) shown in Chart 1 (b), (d), (e), the photoisomerization of *p*-HMC proceeds *via* "$^1\pi\pi^*$ (*trans*) → → T_1 ($^3\pi\pi^*$) → S_0 (*trans* or *cis*)" route, while in *m*- and *o*-HMC, the photoisomerization proceeds *via* "$^1\pi\pi^*$ (*trans*) → C=C bond twisting on the $^1\pi\pi^*$ → S_0 (*trans* or *cis*)" route.[19] Thus, there are at least two photoisomerization routes.

All the above-mentioned results indicate that the photoisomerization of cinnamates is very sensitive to the substitution to phenyl ring. Thus, a systematic theoretical study to track the possible reaction routes starting from the initial photoexcited state (*trans*-form) to the reactant (isomerization to the *cis*- form) or going back to the ground state of the original form, as well as the effect of substitution is highly demanded. In the present study, we carried out a theoretical calculation to answer this demand.

In the first half of the present study, we describe the systematic exploration of the photoisomerization route of MC by using the single-component artificial force induced reaction (SC-AFIR) method with time dependent density functional theory (TD-DFT) calculation, which was successfully applied in drawing the complete photoisomerization route of cinnamates in our previous study.[18,19] Here, we found that the route of MC is essentially described as "$^1\pi\pi^*$ (*trans*) → $^1n\pi^*$ → T_1 ($^3\pi\pi^*$) → S_0 (*trans* or *cis*)". This route becomes important baseline to investigate the substitution effect on the electronic states and the photoisomerization route of cinnamates.

In the latter part, we discuss a prominent guideline to design efficient substituted cinnamate based sunscreens by using the results of the $^1\pi\pi^*$ lifetime, and the shapes and energies of the molecular orbitals (MOs) involved in the $^1\pi\pi^*$ and $^1n\pi^*$ transitions of cinnamates. Here, we found that for the efficient sunscreen, cinnamate should have an appropriate substituent at phenyl ring to stabilize the highest occupied π orbital. We also describe the reason of the modulation of photoisomerization route by substitutions based on these MO concepts.

2. Theoretical calculations

2. 1 Systematic exploration of the photoisomerization route

For the systematic exploration of the photoisomerization routes, we perform DFT and TD-DFT calculations with the development version of the GRRM program[55] interfaced with the Gaussian 16 quantum chemistry package[56] otherwise mentioned.

First, the IC route from the $^1\pi\pi^*$ state is investigated. The $^1\pi\pi^*$ and $^1n\pi^*$ minima (EQs), and the transition state (TS) between them are optimized at the TD-ωB97XD/6-311G(d,p) level. The functional

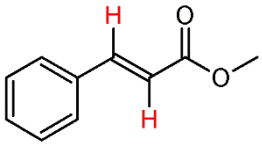

Chart 2. The target atoms for SC-AFIR method: All the carbon atoms, oxygen atoms and hydrogen atoms (indicated as red) in the vinyl C=C bond.

was used in previous studies and it successfully described the energy of the electronic states and NRD process of cinnamates.[19,21]

Next, the intersystem crossing (ISC) route from the $^1n\pi^*$ state is investigated. Minimum energy seams of crossings (MESXs) between the S_1 ($^1n\pi^*$ or $^1\pi\pi^*$) and T_n (n = 2, 3) states are optimized at the TD-ωB97XD/6-311G(d,p) level. The minimum energy conical intersections (MECIs) between the T_2 and T_1 states are searched by the SC-AFIR method[57-60] at the TD-ωB97XD/6-311G(d,p) level. The EQs of T_1 ($^3\pi\pi^*$) and the MESXs between T_1 ($^3\pi\pi^*$) and S_0 are also searched at the UωB97XD/6-31G(d) level. The MECI/MESX search using the SC-AFIR method can investigated much larger configurational space than manual search and gives us surprising number of MECI structures. For example, we found 56 S_1/S_0 MECIs for *o*-HMC in previous study.[19] We have already been applied this method successfully for the nonradiative processes in many organic and inorganic systems and obtained the low-lying MECIs/MESXs involved in their nonradiative decay processes.[18,58-65]

For the investigation of the direct isomerization route, which is C=C rotation coordinate on the $^1\pi\pi^*$ state, we also optimized the geometries of $^1\pi\pi^*/S_0$ MECIs and TSs on the $^1\pi\pi^*$ state. We applied the energy shift technique[66-68] for the $^1\pi\pi^*/S_0$ MECI to avoid the instability of TD-DFT calculations nearby the MECI. Initial geometries of the MECIs are created by the SC-AFIR at the TD-ωB97XD/6-31G(d) level.

In all the SC-AFIR searches, the model collision energy parameter is set to γ = 100 kJ/mol, and all the carbon atoms, oxygen atoms and hydrogen atoms in the vinyl C=C bond are accounted as the target atoms as shown in Chart 2. All of the obtained EQs in T_1 and T_1/S_0 MESXs are further optimized at the UωB97XD/6-311G(d,p) level, and all the other TS, MESXs, MECIs and EQs are optimized at the TD-ωB97XD/6-311G(d,p) level.

The decay routes for all the optimized structures are surveyed by calculating the intrinsic reaction coordinates (IRCs) and the meta-IRC, where IRC and meta-IRC correspond to the steepest decent path starting from the first-order saddle point and those from non-stationary points, respectively.

2. 2 Spin-Orbit coupling constant

To evaluate the efficiency of the ISC ($^1n\pi^*$ or $^1\pi\pi^*$ → triplet state) process, the spin-orbit coupling constant (SOC) at the optimized MESXs are calculated by using the TD-ωB97XD/6-311G(d,p) level of theory using the Breit-Pauli spin-orbit Hamiltonian with effective charge approximation,[69-71] implemented in the PySOC program.[72,73] It is known that the SOC values evaluated by TD-ωB97XD level of TD-DFT well reproduce those calculated by computationally more demanding multistate complete active space second order perturbation theory (MS-CASPT2).[73] The single-point energy calculation for the SOC evaluation is performed by Gaussian 09 quantum chemistry package.[74]

The SOC constant between T_1 and S_0 states at T_1/S_0 MESXs are evaluated at the MS-CASPT2[75] /ANO-RCC-VTZP[77] level of theory with active space of 10 electrons in 9 orbitals ([10e, 9o]-MS-CASPT2). We use mean field spin-orbit Hamiltonian and SOC between the T_1 and S_0 states.[85] The SOC values are evaluated by using restricted active space state interaction approach.[86] We use OpenMolcas 18.09 quantum chemistry package[75] for the MS-CASPT2 calculations. The detailed description of our MS-CASPT2 calculations is documented in supporting information (SI).

3. Results and Discussion

3.1 The photoisomerization *via* multi-step NRD process of MC

Figure 1 shows the energy diagram of the excited states and the photoisomerization route of MC starting from the *trans* $^1\pi\pi^*$ minima (EQ 1) to the T_1 ($^3\pi\pi^*$) minima (EQ 7 and EQ 8). The values with zero-point vibrational energy (ZPE) correction are also shown in parentheses. The crosses in Figure 1 indicate MECIs or MESXs. We hereafter define the dihedral angles of C-C=C-C and C-C-O-Me as the twisting angle around C=C bond and methoxy group, respectively. According to this definition, the twisting angle around C=C bond for *trans* and *cis* isomers are 180° and 0°, respectively.

We found that the UV excited *trans*-MC in $^1\pi\pi^*$ with low excess energy rapidly decays to the triplet states and either goes back to the *trans*-S_0 or undergoes *trans* → *cis* isomerization as same as *para* substituted cinnamates such as *p*-MMC and *p*-HMC.[18,19] Briefly, As seen in Figure 1, this NRD process starts with the IC to $^1n\pi^*$ state followed by ISC to the triplet manifold, first to the T_3 ($^3\pi\pi^*$) state. After this ISC, MC relaxes to T_2 ($^3\pi\pi^*$) by IC. OMe torsion in the T_2 state changes the character to $^3n\pi^*$ and promotes IC to T_1 ($^3\pi\pi^*$) state. MESX between the $^1n\pi^*$ and T_3 ($^3\pi\pi^*$) states (MESX 1) was found near EQ 2. The experimental observation suggests the IC process within the triplet states completes within 1 ns.[18,19,21] In Figure 2, the energy of T_1 and ISC routes to S_0(*trans*) and S_0(*cis*), isomerization route, are shown. The stable structure of the T_1 state has the C=C twisted form, which is close to the T_1/S_0 MESXs. Experimentally, MC in T_1 finally undergoes a few tens of nanoseconds ISC to the S_0 states of *trans* or *cis* form. Hereafter, we will closely look at each NRD steps.

The first IC from $^1\pi\pi^*$ (EQ 1) to $^1n\pi^*$(EQ 2) immediately occurs through the nonplanar avoided crossing type transition state (TS 1) at 35805 cm^{-1}. This IC is a barrier-less process since the energy of TS 1 with zero-point energy correction (34294 cm^{-1}) is lower than that of EQ 1 (34827 cm^{-1}). This explains very well the observation of the very short (4.5 ps) lifetime of the $^1\pi\pi^*$ state in the gas-phase.[15, 21] The planer $^1\pi\pi^*/^1n\pi^*$ MECI 1 was found at 36481 cm^{-1}. However, MECI 1 is energetically higher than that *via* TS 1 by 676 cm^{-1} and MECI 1 dose not much involved in this IC process.

MC next undergoes ISC to the T_3 ($^3\pi\pi^*$) state. MESX 1 is found at 35091 cm^{-1} near EQ 2. The energy of MESX 1 is lower than other MESXs, and the calculated SOC value at MESX 1 (24 cm^{-1}) is large enough for ISC to occur *via* MESX 1. The energies and SOC values of other MESXs are shown in Figure S1 and listed in Table S1. MC in T_3

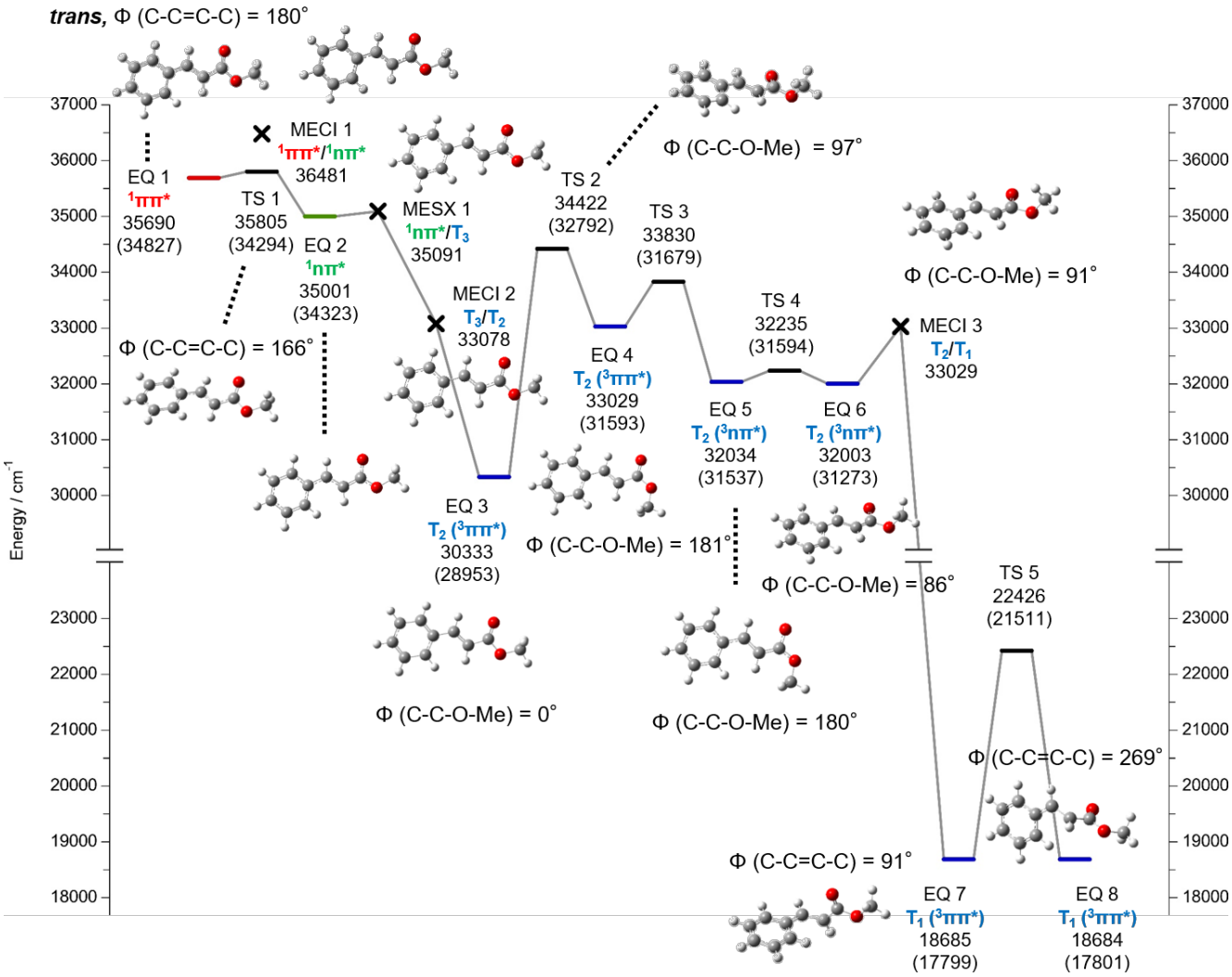

Figure 1. The energy diagram along the decay routes of the photoisomerization of MC from the *trans* $^1\pi\pi^*$ minima (EQ 1) to the T_1 ($^3\pi\pi^*$) minima (EQ 7 and EQ 8) calculated at the ωB97XD/6-311G(d,p) level. The values in parentheses are the ZPE corrected ones. The angles in the structures are the tilting angle of the propenyl C=C bond with respect to the planar structure (*trans*-form). The crosses indicate MECIs or MESXs.

immediately decays to T_2 ($^3\pi\pi^*$) by IC *via* MECI 2 since the IRC from MESX 1 to the T_3 state directly reaches to MECI 2.

After the IC to the T_2 ($^3\pi\pi^*$) state, the OMe group starts tilting. This OMe tilting changes the character of the T_2 from $^3\pi\pi^*$ to $^3n\pi^*$ by passing through an avoided crossing type TS 3 as same as the IC from $^1\pi\pi^*$ to $^1n\pi^*$ (TS 1) discussed above. The OMe torsion further triggers IC to T_1 ($^3\pi\pi^*$) and MC reaches to the C=C twisted T_1 structure (EQ 7). This multistep IC process from T_3 to T_1 completes within a few ns according to our previous nanosecond UV-DUV pump-probe measurement, where only EQ 7 (T_1) is experimentally detected.[21] The 0-0 energy level of EQ 7 is 17799 cm^{-1}, which reasonably agrees with the experimental value (21790 cm^{-1}).[21] The C=C bond in EQ 7 is twisted by 91°, and EQ 7 looks like the TS between *trans* and *cis* isomers. EQ 7 of MC has large excess energy (17028 cm^{-1}) so that it can further isomerize to another T_1 minima (EQ 8) through TS 5. The C=C bond in EQ 8 is twisted by 269°.

We also investigated the other $T_2 \rightarrow T_1$ IC channels apart from the route *via* MECI 3. We found that the MECI 3 is the most energetically preferable T_2/T_1 as shown in Figures 1 and S2. The OMe tilted T_1/T_2 MECI like MECIs 3 and 5 is also energetically preferable for *p*-MMC.[18] However, several other $T_2 \rightarrow T_1$ IC routes involving T_2/T_1 MECIs, described in Figure S2 and S3 in SI *etc.*, are possible because of the large excess energy at the T_2 EQ 3 (5874 cm^{-1}) and the high energy barrier for the OMe tilting (TS 2, 3839 cm^{-1}). The calculated reaction rate for the rate-determining step from EQ 3 to 4 (1.44×10^7 s^{-1}, time constant of 69.4 ns) by using Rice-Ramsperger-Kassel-Marcus (RRKM) theory,[87] assuming the 0-0 transition from the S_0 to $^1\pi\pi^*$ (excess energy at EQ 3 is 5874 cm^{-1}), supports this multiple reaction pathway picture for the T_2/T_1 IC process.

The final step of the multistep ISC is the ISC from the T_1 ($^3\pi\pi^*$) to S_0 state as shown in Figure 2. We found two low-lying T_1/S_0 MESXs, MESX 2 and 3, as shown in the figure. The calculated SOC value at the [10e,9o]-MS-CASPT2/ANO-RCC-VTZP of MESX 2 and MESX 3 is 0.38 and 0.30 cm^{-1}, respectively. According to our *meta*-IRC analysis from these two MESXs, formation of S_0 *trans* form *via* the lower-lying

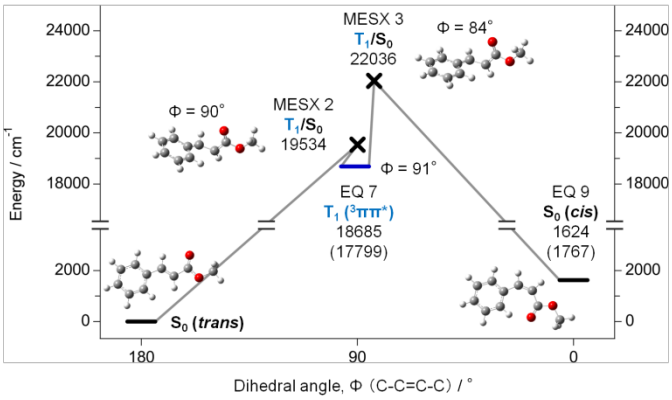

Figure 2. The energy diagram and decay routes of isomerization to *cis* (EQ 9) and going back to *trans* from EQ 7 (T_1, $^3\pi\pi^*$). The x-axis represents the dihedral angle around C=C bond. The angle of *trans*-form is defined as 180°.

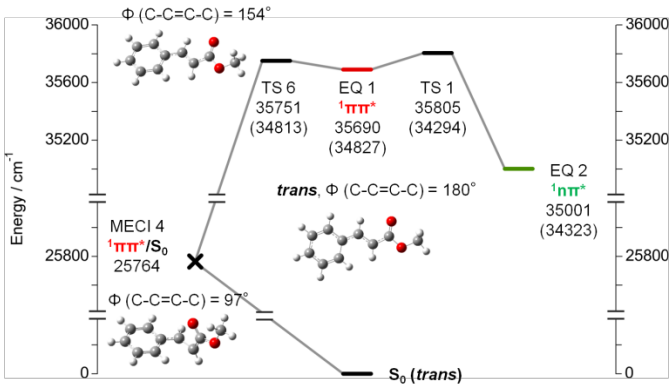

Figure 3. Two competing photoisomerization routes of MC from EQ 1 ($^1\pi\pi^*$). Left direction represents the direct photoisomerization process on the $^1\pi\pi^*$ PES and right direction represents the IC (EQ 1 → EQ 2) process

MESX 2 seems to be energetically more favorable than that of *cis*-form (EQ 9) *via* the higher lying MESX 3.

The $^1\pi\pi^*$ state decays to $^1n\pi^*$ (EQ 2) less than 10 ps according to previous experimental studies.[15,21] The time-resolution of our UV-DUV pump-probe measurement is 6-7 ns and we concluded that the transient state (T_1) is produced faster than this time resolution.[21] Thus, the decay process from EQ 1 to EQ 7 involving ISC *via* MESX 1 occurs within a few ns. The calculated SOC values of T_1/S_0 MESXs 2 and 3 (0.38 and 0.30 cm^{-1}, respectively) is approximately 100 times smaller than that of $^1n\pi^*/^3\pi\pi^*$ MESX 1 (24 cm^{-1}). Thus, the ISC from T_1 to S_0 state is much slower and EQs 7 and 8 can be observed by our UV-DUV pump-probe measurement.

In the gas phase condition such as in a supersonic beam, the MC at the T_1 state has large excess energy of 17028 cm^{-1}. This large excess energy can drive MC to (i) ISC *via* non-IRC pathways (*cis* formation *via* MESX 2 and *trans* formation *via* MESX 3), and (ii) conformation change in the T_1 state, and (iii) *trans* ⇄ *cis* isomerization in the S_0 state after the ISC. On the other hand, in solution the collisional cooling will interrupt the isomerization process. Actually, as was described in introduction, Shindo *et al.* reported the quantum yield (ϕ) for the isomerization of ethyl cinnamate (EC) in ethanol solution is ϕ (*trans* → *cis*) = 0.26 and ϕ (*cis* → *trans*) = 0.29, and suggested that the half of the photoexcited species directly deactivates to S_0 of the same isomeric form.[14] For the determination of the branching ratio of *trans* / *cis* isomerization *via* the multistep ISC, a detailed nonadiabatic kinetics study including these three effects is essential.

We also investigated another multistep ISC pathway that MC directly undergoes ISC from the $^1\pi\pi^*$ to triplet states as suggested by our group[18] and by Moon *et al.*[50] in *p*-MMC. However, we found that this pathway plays a very minor role for the decay of the $^1\pi\pi^*$ state in the case of MC. The character of the all low-lying MESXs around $^1\pi\pi^*$ EQ 1 is $^1\pi\pi^*/^3\pi\pi^*$, where ISC is not preferable according to El-Sayed's rule as shown in Figure S1. As a result, the value of SOC is too small (< 1 cm^{-1}) to explain the experimentally observed decay of the $^1\pi\pi^*$ state within 10 ps (Table S1).

3.2 The photoisomerization *via* C=C bond twisting process on the $^1\pi\pi^*$ PES of MC

Several previous theoretical studies investigated the direct *trans* → *cis* isomerization route *via* $^1\pi\pi^*/S_0$ since it is essential to examine the competition between this route and the $^1\pi\pi^*$ → $^1n\pi^*$ IC for gaining overall picture of the photoisomarization.[17-19,51-53] Here, we also examined the direct $^1\pi\pi^*$ isomerization pathway for MC. We found that in the gas phase the multi-step photoisomerization route *via* IC and ISC discussed in a previous section is preferable than the direct C=C bond twisting on the $^1\pi\pi^*$ PES.

Figure 3 shows the two competing NRD routes connected to photoisomerization from the $^1\pi\pi^*$ minimum (EQ 1) of MC. The right direction from EQ 1 is IC to $^1n\pi^*$ state (EQ 2) discussed above and the left direction is the decay route along the C=C bond twisting on the same $^1\pi\pi^*$ PES. We found TS 6 at 35751 cm^{-1}, located between EQ 1 and $^1\pi\pi^*/S_0$ MECI 4. The TS 6 is the result of the avoided crossing between the first and second $^1\pi\pi^*$ states,[54] which consist of several π → π* configurations such as HOMO (π) → LUMO (π*), HOMO-1 (π) → LUMO (π*) (See Figure 5 and Table S3) *etc*. The MOs involved in these states are originated from the π and π* orbitals of benzene ring and propenyl group as shown in Figure 5. The weight of these π → π* configurations changes according C=C twisting and makes the avoided crossing TS 6. After the IC (MECI 4 → S_0), *trans* → *cis* isomerization will occur in S_0 due to the large excess energy even though the IRC calculation from MECI 4 reaches to S_0 of *trans* form. The ZPE-corrected energy of TS 1 is lower than that of TS 6 by 519 cm^{-1}. This indicates that the $^1\pi\pi^*$ → $^1n\pi^*$ IC route (right direction) is energetically more favorable than that of C=C bond twisting route *via* $^1\pi\pi^*/S_0$ MECI. This theoretical result consists with the experimental result that the T_1 ($^3\pi\pi^*$) corresponds to EQ 7 was detected by nanosecond UV-DUV pump-probe measurement.[21]

3.3 Substitution and its position effect on the NRD process: For the effective NRD of the photoexcited $^1\pi\pi^*$ state

We found that for the efficient IC of the $^1\pi\pi^*$ state, the cinnamate should have an appropriate substituent at the phenyl ring to stabilize highest occupied π orbital. The stabilized π orbital (i) minimizes the energy gap between $^1\pi\pi^*$ and $^1n\pi^*$ at the $^1\pi\pi^*$ minimum, and (ii) makes the 0-0 energy level of $^1\pi\pi^*$ higher than $^1n\pi^*$ state as observed in MC. These MC-like energetic relationships between $^1\pi\pi^*$ and $^1n\pi^*$ should be ideal to maximize the "$^1\pi\pi^*$ → $^1n\pi^*$" IC rate

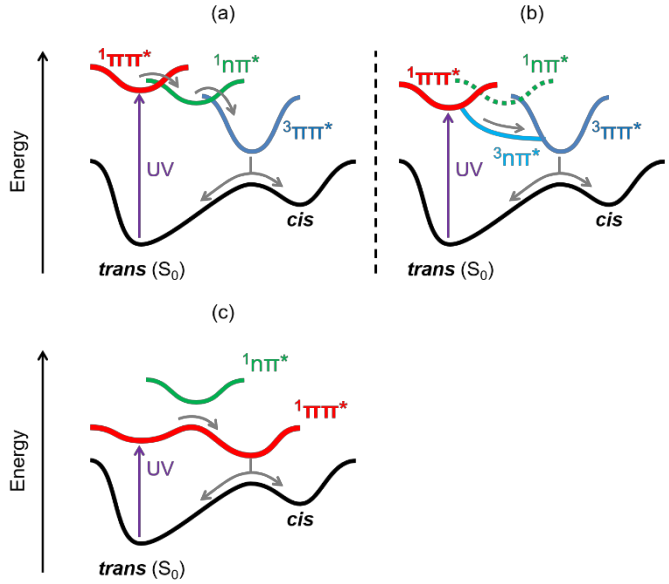

Figure 4. The schematic potential curves of the electronic states along the photoisomerization coordinate for (a) MC, (b) *p*-HMC, *p*-MMC and (c) *m*- and *o*-HMC, respectively. In the routes of (a) and (b), the transient T_1 ($\pi\pi^*$) state is mediated. On the other hand, in the (c) route, the isomerization occurs on the $^1\pi\pi^*$.

constant according to Marcus theory. In this section, we will closely look at how substitution varies the energies of molecular orbitals, and modulates the energy level of $^1\pi\pi^*$ state and NRD mechanism.

3.3.1 *para*-substituted MC

The $^1\pi\pi^*$ lifetime of *para*-substituted cinnamates is also very short meaning the efficient initial NRD ($^1\pi\pi^* \rightarrow {}^1n\pi^*$ and/or $^1\pi\pi^* \rightarrow {}^3n\pi^*$).[18,19,21] This suggests that *para*-substituted cinnamates can be good UV filters if they effectively go back to S_0 or isomerize to the *cis* (*Z*)-form with high yields. Figure 4 shows the schematic potential curves of the electronic states along the photoisomerization coordinate for (a) MC, and for (b) *p*-HMC and *p*-MMC. The substitution of the OH or OCH_3 group at *para* position of MC slightly lowers the $^1\pi\pi^*$ transition energy and elongates the $^1\pi\pi^*$ lifetime, but triplet mediated isomerization process is still dominant. [18,19,21]

Table 1 lists the 0-0 transition energies of the $^1\pi\pi^*$ and $^1n\pi^*$ states ($E_{0\text{-}0}$ ($^1\pi\pi^*$) and $E_{0\text{-}0}$ ($^1n\pi^*$)) calculated at the ωB97XD/6-311G(d,p) level of theory, which are compared to the observed values. Although the calculated energies are roughly 1000 cm^{-1} higher than the observed ones, they show a good agreement for the relative energies of the two states. The calculated results show that the substitution at the *para* position lowers $E_{0\text{-}0}$ ($^1\pi\pi^*$) but less affects $E_{0\text{-}0}$ ($^1n\pi^*$). The calculated $E_{0\text{-}0}$ ($^1n\pi^*$) values of MC, *p*-HMC and *p*-MMC are located within the range of 420 cm^{-1}, while the energy of $^1\pi\pi^*$ is lowered by 1459 cm^{-1} from MC to *p*-MMC, in good agreement with the experimental value of 1632 cm^{-1}. Especially, the order of the two states is reversed between MC and *para*-substituted MC.

Since the IC from the $^1\pi\pi^*$ to $^1n\pi^*$ states involves the hole transfer from the *n* (HOMO-1 or HOMO-2) orbital on carbonyl group to the π (HOMO) orbital as shown in Figure 5, the IC rate constant k_{IC} can be described approximately by Marcus theory,[88]

$$k_{IC} = 2\pi/\hbar \, |H_{1\pi\pi^*\text{-}1n\pi^*}|^2 (4\lambda k_B T)^{-1/2} \times \exp[-(\lambda \rightarrow \Delta G_{1\pi\pi^*\text{-}1n\pi^*})^2 / 4\lambda k_B T], \quad (1)$$

where $H_{1\pi\pi^*\text{-}1n\pi^*}$, λ, and $\Delta G_{1\pi\pi^*\text{-}1n\pi^*}$ are the nonadiabatic coupling between the $^1\pi\pi^*$ to $^1n\pi^*$ states, reorganization energy of the $^1n\pi^*$ state, and free energy difference between the $^1\pi\pi^*$ and $^1n\pi^*$ state, respectively. Under the low temperature (T ~ 10 K) with low-excess energy experimental condition in gas-phase as our previous studies,[16-23] the entropy contributions to λ, and $\Delta G_{1\pi\pi^*\text{-}1n\pi^*}$ eq (1) becomes negligible and is rewritten as the difference of the potential energies,

$$k_{IC} = 2\pi/\hbar \, |H_{1\pi\pi^*\text{-}1n\pi^*}|^2 (4\lambda k_B T)^{-1/2} \times \exp[-(\lambda \rightarrow E_{0\text{-}0}(^1n\pi^*) - E_{0\text{-}0}(^1\pi\pi^*))^2 / 4\lambda k_B T]. \quad (2)$$

Here, λ is approximated by the sum of $|E_{0\text{-}0}(^1n\pi^*) - E_{0\text{-}0}(^1\pi\pi^*)|$ and energy difference between $^1n\pi^*$ and $^1\pi\pi^*$ states U ($^1n\pi^*$- $^1\pi\pi^*$) at $^1\pi\pi^*$ EQ is shown as in Figure 6. The effective activation energy E^* for the IC process can be written as

Table 1. Adiabatic energies of the $^1\pi\pi^*$ and $^1n\pi^*$ states, the $^1\pi\pi^*$ state lifetime and major NRD route of MC and substituted MC

	Calc. (ωB97XD/6-311G(d,p))		Exp.			
Molecule	$E_{0\text{-}0}$ ($^1\pi\pi^*$) / cm^{-1}	$E_{0\text{-}0}$ ($^1n\pi^*$) / cm^{-1}	$E_{0\text{-}0}$ ($^1\pi\pi^*$) / cm^{-1}	τ_1 ($^1\pi\pi^*$) / ps	$E_{0\text{-}0}$ ($^1n\pi^*$) / cm^{-1}	Major NRD route
MC	34827 [a]	34323 [a]	33960 [a]	≤ 10 [a], 4.5 [b]	33300 [a]	$^1\pi\pi^* \rightarrow {}^1n\pi^* \rightarrow {}^3\pi\pi^* \rightarrow S_0$
p-HMC [c]	33697	34692	32710	≤ 10	—	$^1\pi\pi^* \rightarrow {}^3n\pi^* \rightarrow {}^3\pi\pi^* \rightarrow S_0$
p-MMC [d, e]	33368	34743	32328	280	—	$^1\pi\pi^* \rightarrow {}^3n\pi^* \rightarrow {}^3\pi\pi^* \rightarrow S_0$
m-HMC [c]	33243	34178	31390	10000	—	C=C bond twisting on $^1\pi\pi^*$
o-HMC [c]	32763	34280	31200	6000	—	C=C bond twisting on $^1\pi\pi^*$

a) ref. 21, b) ref. 15, c) ref. 19, d) ref. 18, e) ref. 17

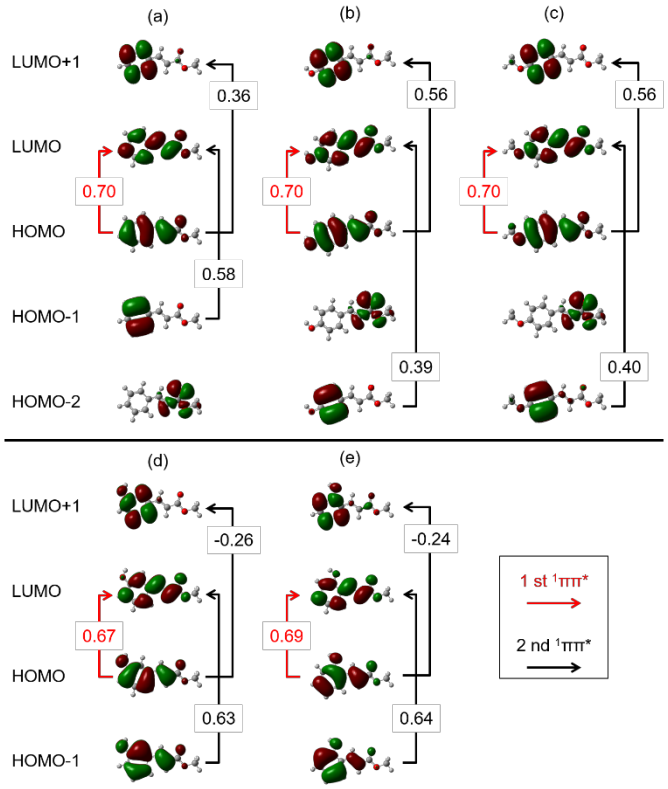

Figure 5. (a)-(c) MOs representing ^{1}nπ* and ^{1}ππ* transitions of MC, *p*-HMC and *p*-MMC, respectively. (d) and (e) MOs representing two types of ^{1}ππ* transition of *m*- and *o*-HMC, respectively. The configuration interaction coefficients obtained by TD-ωB97XD/6-311G(d,p) level of single point calculations at the equilibrium structure of the first ^{1}ππ* state for each molecule are also shown.

$$E^* \equiv \lambda \rightarrow E_{0\text{-}0}(^1\text{n}\pi^*) - E_{0\text{-}0}(^1\pi\pi^*)$$
$$\approx U(^1\text{n}\pi^*\text{-}\,^1\pi\pi^*) + |E_{0\text{-}0}(^1\text{n}\pi^*) - E_{0\text{-}0}(^1\pi\pi^*)|$$
$$+ E_{0\text{-}0}(^1\text{n}\pi^*) - E_{0\text{-}0}(^1\pi\pi^*). \quad (3)$$

Eq. (3) is further simplified by considering the sign of $E_{0\text{-}0}(^1\text{n}\pi^*) - E_{0\text{-}0}(^1\pi\pi^*)$. For $E_{0\text{-}0}(^1\text{n}\pi^*) - E_{0\text{-}0}(^1\pi\pi^*) > 0$,

$$E^* = U(^1\text{n}\pi^*\text{-}\,^1\pi\pi^*) + 2(E_{0\text{-}0}(^1\text{n}\pi^*) - E_{0\text{-}0}(^1\pi\pi^*)). \quad (4a)$$

And for $E_{0\text{-}0}(^1\text{n}\pi^*) - E_{0\text{-}0}(^1\pi\pi^*) \leq 0$,

$$E^* = U(^1\text{n}\pi^*\text{-}\,^1\pi\pi^*). \quad (4b)$$

Eqs. (4a) and (4b) indicate that minimizing $U(^1\text{n}\pi^*\text{-}\,^1\pi\pi^*)$ at ^{1}ππ* EQ and satisfying $E_{0\text{-}0}(^1\text{n}\pi^*) - E_{0\text{-}0}(^1\pi\pi^*) \leq 0$ is a promising strategy to maximize k_{IC} since λ is almost identical for MC, *p*-HMC and *p*-MMC as shown in Table 2. The minimization of $U(^1\text{n}\pi^*\text{-}\,^1\pi\pi^*)$ at ^{1}ππ* EQ can be achieved by (i) destabilizing ^{1}ππ* and/or (ii) stabilizing ^{1}nπ* (Figure 6).

In order to examine which (i) or (ii) is the more feasible, we carefully look at the shapes and energies of MOs associating with the ^{1}ππ* and ^{1}nπ* transitions. Figure 5 (a)-(c) shows four MOs for MC, *p*-HMC and *p*-MMC, respectively. Table 3 lists the energies of LUMO, HOMO and HOMO-2 or HOMO-1 calculated at the ωB97XD/6-311G(d,p) level of theory at the first ^{1}ππ* minimum by Gaussian 09 quantum chemistry package.[74] In these cinnamates, the first ^{1}ππ* and ^{1}nπ* transition corresponds to HOMO → LUMO and HOMO-2 (or HOMO-1) → LUMO transition, respectively. In HOMO of the three molecules, MO is delocalized on the phenyl ring and vinyl group. It should be noted that the substitution of the OH or OCH_3 group at *para* position of MC drastically increases the energy of HOMO by 0.5 eV so that the HOMO-LUMO energy gap of *p*-HMC and *p*-MMC becomes smaller than that of MC. On the other hand, the ^{1}nπ* transition energy is less affected by the substitution (within 0.2 eV), since the nonbonding orbital on the C=O group is far from the substitution point. These changes result in (i) increasing $U(^1\text{n}\pi^*\text{-}\,^1\pi\pi^*)$ at the ^{1}ππ* EQ, and (ii) makes the 0-0 energy level of ^{1}ππ* lower than ^{1}nπ* state. As a result, the ^{1}ππ* → ^{1}nπ* IC rate is reduced in *para*-substituted MC as shown in Table 2 according to Marcus theory, especially in *p*-MMC.

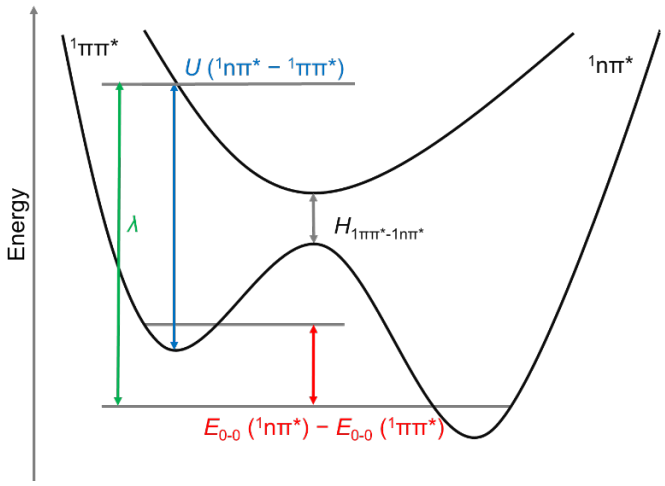

Figure 6 A schematic description of the potential energy curves of MC along the ^{1}ππ* → ^{1}nπ* IC reaction coordinates and the definitions of the parameters appeared in eq (2)

Table 2 Parameters for Marcus equation (2) evaluated at the TD-ωB97XD/6-311G(d,p) level

Molecule	$U(^1\text{n}\pi^*\text{-}\,^1\pi\pi^*)$ /cm^{-1}	$E_{0\text{-}0}(^1\text{n}\pi^*) - E_{0\text{-}0}(^1\pi\pi^*)$/cm^{-1}	λ /cm^{-1}
MC	3690	-594	4284
p-HMC	5457	995	4462
p-MMC	5734	1375	4359

The modulation of the HOMO (π) energy by introducing the substituent is explained by applying Hammett's rule.[89] The correlation between the HOMO energy of the substituted benzene and Hammett σ parameter was already estimated.[90,91] The plots of the HOMO energy against the σ parameters for various substitution groups showed a good correlation. According to those plots, the HOMO of benzene is destabilized by π-donor substitution such as the OH and OCH_3 group. In addition, the HOMO → LUMO transition energy is described by three types of Hammett parameter such as σ_I, σ_π^+ and σ_π^-.[92] Here, σ_I is the inductive substituent constant, while the σ_π^+ and σ_π^- are the π-electronic substituent constants for π-

Table 3 The orbital energies of MC, *p*-HMC and *p*-MMC calculated at the ωB97XD/6-311G(d,p) level at the first $^1\pi\pi^*$ minimum.

Molecule	LUMO (π*) /eV	HOMO (π) /eV	HOMO-1or HOMO-2 (n) /eV	Δ*E* (HOMO-LUMO) / eV	Δ*E* (HOMO-LUMO) / cm^{-1}
MC	-0.645	-8.15	-9.68	7.51	60549
p-HMC	-0.350	-7.71	-9.54	7.36	59331
p-MMC	-0.299	-7.62	-9.50	7.32	59024

donor and π-accepter substituent, respectively. These values for H, OH and OCH_3 groups are listed in Table 4. For example, the transition energy from S_0 to the $^1\pi\pi^*$ state (E^{UV}/eV) for the monosubstituted benzene is described as,[93]

$$E^{UV} = -0.021\sigma_I + 1.194\sigma_\pi^+ - 1.029\sigma_\pi^- + 4.846\,. \qquad (5)$$

The calculated and observed E^{UV} of non-substituted benzene, phenol and anisole are also listed in Table 4.[92-96] This calculated E^{UV} trend consists with experimental values so that it can also be applied to cinnamates.

The experimental results reported in previous studies support the calculated results. The observed $E_{0\text{-}0}$ ($^1\pi\pi^*$), $E_{0\text{-}0}$ ($^1n\pi^*$) and the $^1\pi\pi^*$ lifetime (τ_1) are also listed in Table 1. In the case of MC, the 0-0 transitions of the $^1n\pi^*$ and $^1\pi\pi^*$ states are observed at 33300 cm^{-1} and 33960 cm^{-1}, respectively. The observed $E_{0\text{-}0}$ ($^1n\pi^*$) is located at 660 cm^{-1} lower than that of $^1\pi\pi^*$ state. On the other hand, in neither *p*-HMC nor *p*-MMC, the $^1n\pi^*$ state has not been observed. It is because $E_{0\text{-}0}$ ($^1n\pi^*$) of *p*-HMC and *p*-MMC is higher than $E_{0\text{-}0}$ ($^1\pi\pi^*$) in those species, as indicated by the calculated ones, the transition to this state is overlapped with the vibronic bands of the bright $^1\pi\pi^*$ state so that it is hard to discriminate it. The measured $^1\pi\pi^*$ lifetime at v = 0 level (τ_1) of *p*-MMC is much longer than both of MC and *p*-HMC. The longer $^1\pi\pi^*$ lifetime of *p*-MMC is explained by its larger $^1\pi\pi^*$-$^1n\pi^*$ energy gap.[16,17,21]

The energy difference between $^1\pi\pi^*$ and $^1n\pi^*$ states changes the rate of the IC and activates the another multistep ISC pathway such as "$^1\pi\pi^*$ (*trans*) → T_2 ($^3n\pi^*$) → T_1 ($^3\pi\pi^*$) → S_0 (*trans* or *cis*)" as suggested by our group[18] and by Moon *et al.*[50] as discussed in *p*-MMC previously. Different from MC, the $^3n\pi^*$ state of *p*-HMC and *p*-MMC is located at much higher energy (~3000 cm^{-1}) above the $^1\pi\pi^*$ EQ and below $^1n\pi^*$ as shown in Table S2 in SI. For MC, it satisfies $E_{0\text{-}0}$ ($^1\pi\pi^*$) > $E_{0\text{-}0}$ ($^1n\pi^*$) as shown in Table 1 and fast IC to $^1n\pi^*$ within 10 ps is the major initial process of the multistep ISC. Population of $^1n\pi^*$ is large enough for the direct detection by our picosecond UV-UV pump probe setup.

On the other hands, $E_{0\text{-}0}$ ($^1\pi\pi^*$) of *p*-HMC and *p*-MMC is lower than $E_{0\text{-}0}$ ($^1n\pi^*$). This switches the major NRD route to ISC to $^3n\pi^*$ in the time scale of picoseconds and only the $^3\pi\pi^*$ (T_1) state becomes experimentally observable in *p*-MMC and *p*-HMC.[18,19] The lifetime of the $^1\pi\pi^*$ of *p*-HMC and *p*-MMC should be also affected by the height of $^1\pi\pi^*$/$^3n\pi^*$ MESX, the SOC between $^1\pi\pi^*$ and $^3n\pi^*$ states, and the vibrational density of states of the $^3n\pi^*$ state. The strategy derived from Marcus theory discussed in $^1\pi\pi^*$ → $^1n\pi^*$ IC can also be helpful for improving efficiency of $^1\pi\pi^*$ → $^3n\pi^*$ ISC, which also involves the hole transfer from carbonyl group to phenyl ring.[97]

For further investigation on the substitution effects on the initial step of multistep ISC and subsequent isomerization dynamics, the interplay between pump-probe spectroscopies such as time-resolved photoelectron spectroscopy[15,98] and transient absorption spectroscopy,[15] and nonadiabatic reaction dynamics and spectroscopic studies based on highly accurate wave function based electronic structure methods[99] (eg. MS-CASPT2 using large active space[50], EOM-CCSD, or ADC(3) combined with aug-cc-pVTZ or lager basis set) is desirable.[83] Especially, the T_1 → T_n transient absorption combined with UV-DUV pump-probe spectroscopy with an aid of *ab-initio* calculations on the T_1 → T_n absorption will give us complemental information for the T_1 state we observed in previous studies.[18,19,21] A possible experimental setup and the simulated T_1 → T_n excited state absorption spectra simulated at the [10e,9o]-MS-CASPT2/ANO-RCC-VTZP level of theory are discussed in SI (Scheme S1, Figures S5 and S6) Another method is the observation of the vibrational spectrum of T_1 state combined with UV-DUV pump-probe spectroscopy, which was demonstrated for the study of NRD of thymine by Boldissar *et al*.[84]

3.3.2 *meta*- and *ortho*-substituted MC

Table 4. The values of σ_I, σ_π^+ and σ_π^- of H, OH, OCH_3 group and E^{UV} (cm^{-1}) of the S_0 → $^1\pi\pi^*$ transition of benzene derivatives. Here, the 0-0 transition of benzene is forbidden so that experimentally predicted value is listed.

				Calc.		Exp.
Substitution	σ_I	σ_π^+	σ_π^-	E^{UV} / eV	E^{UV} / cm^{-1}	E^{UV} / cm^{-1}
H (benzene) [a, b, c]	0	0	0	4.85	39086	38086
OH (phenol) [a, b, d]	0.190	-0.340	0	4.44	35779	36348
OCH_3 (anisole) [a, b, e]	0.185	-0.281	0	4.51	36348	36384

a) ref. 92, b) ref. 93, c) ref. 94, d) ref. 95 e) ref. 96

The substitution of the OH group at *meta* or *ortho* position of the phenyl ring of MC further lowers the $^1\pi\pi^*$ transition energy and drastically elongates the $^1\pi\pi^*$ lifetime. As a result, as shown in Figure 4 (c) the substitution at these positions changes the dominant NRD / photoisomerization route of MC to C=C bond twisting on the $^1\pi\pi^*$ PES described as "$^1\pi\pi^*$ (*trans*) → C=C bond twisting on $^1\pi\pi^*$ → S_0 (*trans* or *cis*)".

As discussed in section 3.2 for MC, the first and second $^1\pi\pi^*$ states ($^1\pi\pi^*$ (1) and $^1\pi\pi^*$ (2), respectively) of cinnamates are originated from several π → π* configurations such as HOMO (π) → LUMO (π*), HOMO-1 (π) → LUMO (π*) and HOMO (π) → LUMO+1 (π*) where the weight of these configuration is different in the $^1\pi\pi^*$ (1) and $^1\pi\pi^*$ (2) states as shown in Table S3. The shape of molecular orbitals is summarized in Figure 5. The energies of the $^1\pi\pi^*$ (1) and $^1\pi\pi^*$ (2) states depend on the substitution position due to the different strength of configuration interaction between them.[42] As a result, although the $^1\pi\pi^*$ (1) and $^1\pi\pi^*$ (2) splitting is small in MC and *p*-HMC, the energy level of $^1\pi\pi^*$ (1) of *m*- and *o*-HMC becomes significantly lower than that of MC. As seen in Table 1, the calculated $E_{0\text{-}0}$ ($^1\pi\pi^*$) of *m*- and *o*-HMC is lower than that of MC and *para*-substituted MC. This is in accordance with the observed $E_{0\text{-}0}$ ($^1\pi\pi^*$) of *m*- and *o*-HMC to be 2570 and 2760 cm^{-1} lower than that of MC, respectively, and more than 1000 cm^{-1} lower than those of the *para*-substituted MC. The magnitude of the lowering of the calculated $^1\pi\pi^*$ transition energy seems to be underestimated for *m*- and *o*-HMC. The calculated $E_{0\text{-}0}$ ($^1n\pi^*$) of *m*- and *o*-HMC is not drastically changed compared to $E_{0\text{-}0}$ ($^1\pi\pi^*$); almost same with those of MC and *para*-substituted MC (Table 1).

The mixture of HOMO (π) → LUMO (π*), HOMO-1 (π) → LUMO (π*) and HOMO (π) → LUMO+1 (π*) transitions is characteristic to the electronic states in *meta* or *ortho*-disubstituted benzene, the reduction of symmetry causes extensive configuration interaction between pure transitions and the interaction results in the larger splitting of the energy levels, where the splitting for *ortho* is slightly larger than that of *meta*. Same patterns of the two $^1\pi\pi^*$ transitions and MOs were also reported for the structural isomers of HMC and other cinnamates by using the symmetry-adapted cluster configuration interaction method, and two distinct $^1\pi\pi^*$ transitions were observed at the absorption spectra of *meta* and *ortho*-cinnamate derivatives and aminostilbene.[42-44,100]

As the experimental results, the drastically long $^1\pi\pi^*$ lifetime of *m*- and *o*-HMC, longer by factor of 1000 than that of MC, is attributed to the inhibition of the $^1\pi\pi^*$ → $^1n\pi^*$ IC and $^1\pi\pi^*$ → $^3n\pi^*$ ISC routes due to their larger energy barrier than that of MC and *para*-substituted MC. As another example, it is reported that the 0-0 transitions of jet-cooled *meta* and *ortho*-diethynylbenzene appear at lower energy than that of *para*.[101]

4. Conclusions

In this study, we theoretically found that for the efficient sunscreen UV filter, the cinnamate should have appropriate substituent at phenyl ring to stabilize the highest occupied π orbital. Stabilization of the π orbital (i) minimizes the energy gap between $^1\pi\pi^*$ and $^1n\pi^*$ at the $^1\pi\pi^*$ minimum, and (ii) makes the 0-0 energy level of $^1\pi\pi^*$ higher than $^1n\pi^*$ state as observed in MC. These MC-like energetic relationships between $^1\pi\pi^*$ and $^1n\pi^*$ should be ideal to maximize the $^1\pi\pi^*$ → $^1n\pi^*$ IC rate constant according to Marcus theory. The substitution effects on the electronic structure and NRD of the phenyl ring were discussed in comparison with non-substituted cinnamate, MC and substituted MC.

The NRD process involving the *trans* (*E*) → *cis* (*Z*) photoisomerization of MC have been theoretically revealed by the SC-AFIR method combined with DFT and TD-DFT calculations at the ωB97XD/6-311G(d,p) level. The calculation showed that the efficient $^1\pi\pi^*$ → $^1n\pi^*$ IC process is energetically favorable than the C=C bond twisting process on the $^1\pi\pi^*$ PES. Therefore, the dominant photoisomerization route of MC is concluded as "$^1\pi\pi^*$ (*trans*) → $^1n\pi^*$ → T_1 ($^3\pi\pi^*$) → S_0 (*trans* or *cis*)".

The substitution effect on the NRD / photoisomerization route of cinnamates has been further examined with focusing on the relationship between the experimentally observed $^1\pi\pi^*$ lifetime, and the shapes and energies of the molecular orbitals (MOs) related with the $^1\pi\pi^*$ and $^1n\pi^*$ transitions of cinnamates. The substitution at *para* position destabilize HOMO (π) and lowers the energy of the $^1\pi\pi^*$ state of MC, so that the order of $^1\pi\pi^*$ and $^1n\pi^*$ state is reversed between MC and *para*-substituted MC. This energy inversion increases the contribution of another sub-nanosecond NRD route involving T_1 ($^3\pi\pi^*$): $^1\pi\pi^*$ (*trans*) → $^3n\pi^*$ → T_1 ($^3\pi\pi^*$) → S_0 (*trans* or *cis*). For *meta* and *ortho* substituted cinnamates (*m*- and *o*-HMC), the energy level of $^1\pi\pi^*$ is more significantly lowered and energy barrier of IC ($^1\pi\pi^*$ → $^1n\pi^*$) becomes very high. As the results, the direct nanosecond photoisomerization process twisting C=C bond on the $^1\pi\pi^*$ PES becomes the dominant photoisomerization route in *m*- and *o*-HMC. These results indicate that the substitution to the phenyl ring drastically changes the photochemistry of the cinnamates, but the modification of the ester part is less effective. An efficient substituted cinnamate based sunscreen should therefore have appropriate substituent at the phenyl ring namely at *para* position to stabilize the highest occupied π orbital and enhance the $^1\pi\pi^*$ → $^1n\pi^*$ IC.

The present study systematically analyzed the substitution effect on the electronic states and the NRD / photoisomerization route of cinnamate derivatives with a substituent on the phenyl ring and revealed that *para*-substituted cinnamates can be the most effective sunscreen reagents because the multistep ISC process can rapidly convert the harmful absorbed UV energy to safety thermal one.

The solvation effect, deprotonation, and protonation are the other important issues for designing of more practical sunscreen reagents, although it has not revealed in this study. For the solvation effect, the laser spectroscopic study on the jet-cooled micro solvated cluster (1:1 complex with solvent molecule) suggests that H-bonding between cinnamate and solvated molecule also drastically affects the NRD process of cinnamate.[16,17,21,23,26-28] Deprotonation of cinnamic acid based sunscreens such as coumaric and ferulic acids drastically changes the mechanism and rate constant of photoisomerization.[45-49] Deprotonation and protonation also perturb the photochemistry of the other sunscreens: Protonation and deprotonation affects the photofragmentation dynamics of oxybenzene sunscreens.[102] Protonation to avobenzone UV-A sunscreen significantly disrupts the stability of the UV-A active enol tautomer for enol to keto photoisomerization.[103] For understanding these effects, additional theoretical study, namely systematic reaction pathway search that we performed in this study and

nonadiabatic reaction dynamics study based on highly accurate wave function based electronic structure methods, will be necessary.

Conflicts of interest

The authors declare no competing financial interest.

Acknowledgements

T. E. acknowledges the financial support from the Institute for Quantum Chemical Exploration and Ministry of Science and Technology, Taiwan for a visiting professorship (grant No. MOST 108-2811-M-009-508). K. Y. is grateful for the financial support from Building of Consortia for the Development of Human Resources in Science and Technology, MEXT. M. E. acknowledges Grants-in-Aid for Scientific Research by JSPS (Nos. JP16H06511 and JP20H02718). Y. H. was supported by JST, PRESTO with grant number JPMJPR16N8. S. M. was supported by JST, CREST with grant number JPMJCR14L5. This work was partly supported by JSPS KAKENHI Grant Number JP20H00374 (Y. I.). Part of the calculations in this paper was carried out by using the supercomputers at Academic Center for Computing and Media Studies, Kyoto University and Okazaki Research Facilities (Research Center for Computational Science).

Notes and references

1 R. Shuab, R. Lone and K.K. Koul, *Acta. Physiol. Plant,* 2016, **38**, 64.
2 J. Luo, Y. Liu, S. Yang, A. L. Flourat, F. Allais and K. Han, *J. Phys. Chem. Lett.*, 2017, **8**, 1025-1030.
3 X. Zhao, J. Luo, S. Yang and K. Han, *J. Phys. Chem. Lett.*, 2019, **10**, 4197-4202.
4 X. Zhao, J. Luo, Y. Liu, P. Pandey, S. Yang, D. Wei and K. Han, *J. Phys. Chem. Lett.*, 2019, **10**, 5244-5249.
5 H. Kuramochi, S. Takeuchi and T. Tahara, *J. Phys. Chem. Lett.*, 2012, **3**, 2025-2029.
6 H. Kuramochi, S. Takeuchi, K. Yonezawa, H. Kamikubo, M. Kataoka and T. Tahara, *Nat. Chem.*, 2017, **9**, 660-666.
7 R. Lone, R. Shuab and K. K. Koul, *Global. J. Phama.*, 2014, **8**, 328-335.
8 N. Serpone, A. Salinaro, A. V. Emeline, S. Horikoshi, H. Hidaka and J. Zhao, *Photochem. Photobiol. Sci.*, 2002, **1**, 970-981.
9 A. Sharma, K. Bányiová, P. Babica, N. E. Yamani, A. R. Collins and P. Čupr, *Sci. Total Environ.*, 2017, **593**-**594**, 18-26.
10 B. Danylec and M. N. Iskander, *J. Chem. Educ.,* 2002, **79**, 1000–1001.
11 H. El-Gezawy, W. Rettig, A. Danel and G. Jonusauskas, *J. Phys. Chem. B*, 2005, **109**, 18699-18705.
12 Y. Miyazaki, Y. Inokuchi, N. Akai and T. Ebata, *J. Phys. Chem. Lett.,* 2015, **6**, 1134-1139.
13 R. B. Rodríguez, R. L. Zapata, M. L. Salum and R. Erra-Balsells, *Photochem. Photobiol. Sci.*, 2020, **19**, 819-830.
14 Y. Shindo, K. Horie and I. Mita, *J. Photochem.*, 1984, **26**, 185-192.
15 K. M. Krokidi, M. A. P. Turner, P. A. J. Pearcy and V. G. Stavros, *Mol. Phys.*, 2020, DOI: 10.1080/00268976.2020.1811910.
16 D. Shimada, R. Kusaka, Y. Inokuchi, M. Ehara and T. Ebata, *Phys. Chem. Chem. Phys.,* 2012, **14**, 8999-9005.
17 Y. Miyazaki, K. Yamamoto, J. Aoki, T. Ikeda, Y. Inokuchi, M. Ehara and T. Ebata, *J. Chem. Phys.,* 2014, **141**, 244313.
18 K. Yamazaki, Y. Miyazaki, Y. Harabuchi, T. Taketsugu, S. Maeda, Y. Inokuchi, S. Kinoshita, M. Sumida, Y. Onitsuka, H. Kohguchi, M. Ehara and T. Ebata, *J. Phys. Chem. Lett.,* 2016, **7**, 4001-4007.
19 S. Kinoshita, Y. Miyazaki, M. Sumida, Y. Onitsuka, H. Kohguchi, Y. Inokuchi, N. Akai, T. Shiraogawa, M. Ehara, K. Yamazaki, Y. Harabuchi, S. Maeda, T. Taketsugu and T. Ebata, *Phys. Chem. Chem. Phys.,* 2018, **20**, 17583-17598.
20 S. Kenjo, Y. Iida, N. Chaki, S. Kinoshita, Y. Inokuchi, K. Yamazaki and T. Ebata, *Chem. Phys.*, 2018, **515**, 381-386.
21 S. Kinoshita, Y. Inokuchi, Y. Onitsuka, H. Kohguchi, N. Akai, T. Shiraogawa, M. Ehara, K. Yamazaki, Y. Harabuchi, S. Maeda and T. Ebata, *Phys. Chem. Chem. Phys.*, 2019, **21**, 19755-19763.
22 S. Muramatsu, S. Nakayama, S. Kinoshita, Y. Onitsuka, H. Kohguchi, Y. Inokuchi, C. Zhu and T. Ebata, *J. Phys. Chem. A*, 2020, **124**, 1272-1278.
23 Y. Iida, S. Kinoshita, S. Kenjo, S. Muramatsu, Y. Inokuchi, C. Zhu and T. Ebata, *J. Phys. Chem. A*, 2020, **124**, 5580-5589.
24 M. D. Horbury, E. L. Holt, L. M.M. Mouterde, P. Balaguer, J. Cebrián, L. Blasco, F. Allais and V. G. Stavros, *Nat. Commun.*, 2019, **10**, 4748.
25 M. D. Horbury, A. L. Flourat, S. E. Greenough, F. Allais and V. G. Stavros, *Chem. Commun.,* 2018, **54**, 936-939.
26 E. M. M. Tan, M. Hilbers and W. J. Buma, *J. Phys. Chem. Lett.,* 2014, **5**, 2464-2468.
27 J. Fan , W. Roeterdink and W. J. Buma, *Mol. Phys.*, 2020, DOI: 10.1080/00268976.2020.1825850.
28 E. M. M. Tan, S. Amirjalayer, B. H. Bakker and W. J. Buma, *Faraday Discuss.*, 2013, **163**, 321-340.
29 E. M. M. Tan, S. Amirjalayer, S. Smolarek, A. Vdovin, A. M. Rijs and W. J. Buma, *J. Phys. Chem. B*, 2013, **117**, 4798-4805.
30 S. Smolarek, A. Vdovin, E. M. M. Tan, M. de Groot, W. J. Buma, *Phys. Chem. Chem. Phys.*, 2011, **13**, 4393-4399.
31 S. Smolarek, A. Vdovin, D. L. Perrier, J. P. Smit, M. Drabbels, and W. J. Buma, *J. Am. Chem. Soc.*, 2010, **132**, 6315-6317.
32 L. A. Baker, M. Staniforth, A. L. Flourat, F. Allais and V. G. Stavros, *ChemPhysChem*, 2020, **21**, 2006-2011.
33 J. M. Woolley, J. S. Peters, M. A. P. Turner, G. J. Clarkson, M. D. Horbury and V. G. Stavros, *Phys. Chem. Chem. Phys.*, 2019, **21**, 14350-14356.
34 M. D. Horbury, W.-D. Quan, A. L. Flourat, F. Allais and V. G. Stavros, *Phys. Chem. Chem. Phys.*, 2017, **19**, 21127-21131.
35 N. D. N. Rodrigues, M. Staniforth, J. D. Young, Y. Peperstraete, N. C. Cole-Filipiak, J. R Gord, P. S. Walsh, D. M. Hewett, T. S. Zwier and V. G. Stavros, *Faraday Discuss.*, 2016, **194**, 709-729.
36 L. A. Baker, M D. Horbury, S. E. Greenough, F. Allais, P. S. Walsh, S. Habershon, and V. G. Stavros, *J. Phys. Chem. Lett.*, 2016, **7**, 56-61.
37 M D. Horbury, L. A. Baker, W-D. Quan, S. E. Greenough and V. G. Stavros, *Phys. Chem. Chem. Phys.*, 2016, **18**, 17691-17697.
38 Y. Peperstraete, M. Staniforth, L. A. Baker, N. D. N. Rodrigues, N. C. Cole-Filipiak, W-D. Quana and V. G. Stavros, *Phys. Chem. Chem. Phys.*, 2016, **18**, 28140-28149.
39 J. C. Dean, R. Kusaka, P. S. Walsh, F. Allais and T. S. Zwier, *J. Am. Chem. Soc.*, 2014, **136**, 14780-14795.
40 J. D. Young, M. Staniforth, J. C. Dean, G. M. Roberts, F. Mazzoni, T. N. V. Karsili, M. N. R. Ashfold, T. S. Zwier and V. G. Stavros, *J. Phys. Chem. Lett.*, 2014, **5**, 2138-2143.
41 C. P. Rodrigo, W. H. James and T. S. Zwier, *J. Am. Chem. Soc.*, 2011, **133**, 2632-2641.
42 M. Promkatkaew, S. Suramitr, T. Karpkird, S. Wanichwecharungruang, M. Ehara and S. Hannongbua, *Photochem. Photobiol. Sci.*, 2014, **13**, 583-594.
43 M. Promkatkaew, S. Suramitr, T. M. Karpkird, S. Namuangruk, M. Ehara and S. Hannongbua, *J. Chem. Phys.*, 2009, **131**, 224306.
44 T. M. Karpkird, S. Wanichweacharungruang and B. Ibinsson, *Photochem. Photobiol. Sci.*, 2009, **8**, 1455-1460.
45 A. Espagne, D. H. Paik, P. C. Barret, M. M. Martin, A. H. Zewail, *ChemPhysChem*, 2006, **7**, 1717-1726.
46 J. N. Bull, C. S. Anstöter, and J. R. R. Verlet, *J. Phys. Chem. A,* 2020, **124**, 2140-2151.

47 J. N. Bull, C. S. Anstöter, and J. R. R. Verlet, *Nat. Comm.*, 2019, **10**, 1.
48 J. N. Bull, G. da Silva, M. S. Scholz, E. Carrascosa, and E. J. Bieske, *J. Phys. Chem. A*, 2019, **123**, 4419-4430.
49 S. Wang, S. Schatz, M. C. Stuhldreier, H. Böhnke, J. Wiese, C. Schröder, T. Raeker, B. Hartke, J. K. Keppler, K. Schwarz, F. Renth, and F. Temps, *Phys. Chem. Chem. Phys.* 2017, **19**, 30683-30694.
50 J. Moon, H. Baek, J. S. Lim and J. Kim, *Bull. Korean Chem. Soc.*, 2018, **39**, 427-434.
51 X-Y. Xie, C-X. Li, Q. Fang and G. Cui, *J. Phys. Chem. A*, 2016, **120**, 6014-6022.
52 X-P. Chang, C-X. Li, B-B. Xie and G. Cui, *J. Phys. Chem. A*, 2015, **119**, 11488-11497.
53 T. N. V. Karsili, B. Marchetti, M. N. R. Ashfold and W. Domcke, *J. Phys. Chem. A*, 2014, **118**, 11999-12010.
54 X. Zhao, F. Ji, Y. Liang, P. Li, Y. Jia, X. Feng, Y. Sun, Y. Shi, L. Zhu and G. Zhao, *J. Lumin.*, 2020, **223**, 117228.
55 Maeda, Y. Harabuchi, M. Takagi, K. Saita, K. Suzuki, T. Ichino, Y. Sumiya, K. Sugiyama and Y. Ono, *J. Comput. Chem.*, 2018, **39**, 233-250.
56 Gaussian 16, Revision B.01, M. J. Frisch, G. W. Trucks, H. B. Schlegel, G. E. Scuseria, M. A. Robb, J. R. Cheeseman, G. Scalmani, V. Barone, G. A. Petersson, H. Nakatsuji, X. Li, M. Caricato, A. V. Marenich, J. Bloino, B. G. Janesko, R. Gomperts, B. Mennucci, H. P. Hratchian, J. V. Ortiz, A. F. Izmaylov, J. L. Sonnenberg, D. Williams-Young, F. Ding, F. Lipparini, F. Egidi, J. Goings, B. Peng, A. Petrone, T. Henderson, D. Ranasinghe, V. G. Zakrzewski, J. Gao, N. Rega, G. Zheng, W. Liang, M. Hada, M. Ehara, K. Toyota, R. Fukuda, J. Hasegawa, M. Ishida, T. Nakajima, Y. Honda, O. Kitao, H. Nakai, T. Vreven, K. Throssell, J. A. Montgomery, Jr., J. E. Peralta, F. Ogliaro, M. J. Bearpark, J. J. Heyd, E. N. Brothers, K. N. Kudin, V. N. Staroverov, T. A. Keith, R. Kobayashi, J. Normand, K. Raghavachari, A. P. Rendell, J. C. Burant, S. S. Iyengar, J. Tomasi, M. Cossi, J. M. Millam, M. Klene, C. Adamo, R. Cammi, J. W. Ochterski, R. L. Martin, K. Morokuma, O. Farkas, J. B. Foresman, and D. J. Fox, Gaussian, Inc., Wallingford CT, 2016.
57 S. Maeda, K. Ohno and K. Morokuma, *Phys. Chem. Chem. Phys.*, 2013, **15**, 3683-3701.
58 S. Maeda, T. Taketsugu and K. Morokuma, *J. Comput. Chem.*, 2014, **35**, 166-173.
59 S. Maeda, Y. Harabuchi, T. Taketsugu and K. Morokuma, *J. Phys. Chem. A*, 2014, **118**, 12050-12058.
60 Y. Harabuchi, T. Taketsugu and S. Maeda, *Chem. Phys. Lett.*, 2017, **674**, 141-145.
61 Y. Harabuchi, T. Taketsugu and S. Maeda, *Phys. Chem. Chem. Phys.*, 2015, **17**, 22561-22565.
62 Y. Harabuchi, T. Taketsugu and S. Maeda, *Chem. Lett.*, 2016, **45**, 940-942.
63 K. Saita, Y. Harabuchi, T. Taketsugu, O. Ishitani and S. Maeda, *Phys. Chem. Chem. Phys.*, 2016, **18**, 17557-17564.
64 Y. Harabuchi, K. Saita, S. Maeda, *Photochem. Photobiol. Sci.*, 2018, **17**, 315-322.
65 K. Saita, M. Takagi, Y. Harabuchi, H. Okada and S. Maeda, *J. Chem. Phys.*, 2018, **149**, 072329.
66 Y. Harabuchi, M. Hatanaka, S. Maeda, *Chem. Phys. Lett.: X*, 2019, **2**, 100007.
67 M. Hatanaka, K. Morokuma**,** *J. Chem. Theory Comput.***,** 2014, **10**, 4184**-**4188**.**
68 M. Hatanaka, Y. Hirai, Y. Kitagawa, T. Nakanishi, Y. Hasegawa, K. Morokuma, *Chem. Sci.***,** 2017, **8**, 423-429**.**
69 S. Koseki, M. W. Schmidt and M. S. Gordon, *J. Phys. Chem.*, 1992, **96**, 10768-10772.
70 S. Koseki, M. S. Gordon, M. W. Schmidt and N. Matsunaga, *J. Phys. Chem.*, 1995, **99**, 12764-12772.
71 S. G. Chiodo and N. Russo, *J. Comput. Chem.*, 2009, **30**, 832-839.
72 S. G. Chiodo and M. Leopoldini, *Comput. Phys. Commun.*, 2014, **185**, 676-683.
73 X. Gao, S. Bai, D. Fazzi, T. Niehaus, M. Barbatti and W. Thiel, *J. Chem. Theory Comput.*, 2017, **13**, 515-524.
74 Gaussian 09, Revision D.01, M. J. Frisch, G. W. Trucks, H. B. Schlegel, G. E. Scuseria, M. A. Robb, J. R. Cheeseman, G. Scalmani, V. Barone, B. Mennucci, G. A. Petersson, H. Nakatsuji, M. Caricato, X. Li, H. P. Hratchian, A. F. Izmaylov, J. Bloino, G. Zheng, J. L. Sonnenberg, M. Hada, M. Ehara, K. Toyota, R. Fukuda, J. Hasegawa, M. Ishida, T. Nakajima, Y. Honda, O. Kitao, H. Nakai, T. Vreven, J. A. Montgomery, Jr., J. E. Peralta, F. Ogliaro, M. Bearpark, J. J. Heyd, E. Brothers, K. N. Kudin, V. N. Staroverov, T. Keith, R. Kobayashi, J. Normand, K. Raghavachari, A. Rendell, J. C. Burant, S. S. Iyengar, J. Tomasi, M. Cossi, N. Rega, J. M. Millam, M. Klene, J. E. Knox, J. B. Cross, V. Bakken, C. Adamo, J. Jaramillo, R. Gomperts, R. E. Stratmann, O. Yazyev, A. J. Austin, R. Cammi, C. Pomelli, J. W. Ochterski, R. L. Martin, K. Morokuma, V. G. Zakrzewski, G. A. Voth, P. Salvador, J. J. Dannenberg, S. Dapprich, A. D. Daniels, O. Farkas, J. B. Foresman, J. V. Ortiz, J. Cioslowski, and D. J. Fox, Gaussian, Inc., Wallingford CT, 2013.
75 J. Finley, P.-Å. Malmqvist, B. O. Roos and L. Serrano-Andrés, *Chem. Phys. Lett.*, 1987, **288**, 299-306.
76 I. F. Galván *et al.*, *J. Chem. Theory Comput.*, 2019, **15**, 5925-5964.
77 B. O. Roos, R. Lindh, P.-Å. Malmqvist, V. Veryazov and P.-O. Widmark, *J. Phys. Chem. A*, 2004, **108**, 2851-2858.
78 F. Aquilante, P.-Å. Malmqvist, T. B. Pedersen, A. Ghosh and B. O. Roos, *J. Chem. Theory Comput.*, 2008, **4**, 694-702.
79 P.-Å. Malmqvist, Alistair Rendell and B. O. Roos, *J. Phys. Chem.*, 1990, **94**, 5477-5482.
80 G. Ghigo, B. O. Roos and P.-Å. Malmqvist, *Chem. Phys. Lett.*, 2004, **396**, 142-149.
81 P.-Å. Malmqvist and B. O. Roos, *Chem. Phys. Lett.*, 1989, **155**, 189-194.
82 W. R. Jhang, H. Y. Lai, Y.-C. Lin, C. Lee, S.-H. Lee, Y.-Y. Lee, C.-K. Ni, C.-M. Tseng, *J. Chem. Phys.*, 2019, **151**, 141101.
83 S. Pathak *et al. Nat. Chem.,* 2020, **12**, 795-800.
84 S. Boldissar and M. S. de Vires, *Phys. Chem. Chem. Phys.*, 2018, **20**, 9701-9716.
85 B. A. Heß, C. M. Marian, U. Wahlgren, O. Gropen, *Chem. Phys. Lett.*, 1996, **251**, 365-371.
86 P.-Å. Malmqvist, B. O. Roos, and B. Schimmelpfennig, *Chem. Phys. Lett.*, 2002, **357**, 230-240.
87 R. A. Marcus, *J. Chem. Phys.*, 1952, **20**, 359.
88 R. A. Marcus, *Angew. Chem. Int. Ed.,* 1993, **32**, 1111-1121.
89 C. Hansch, A. Leo and R. W. Taft, *Chem. Rev.*, 1991, **91**, 165-195.
90 H. Fujimoto, K. Sakata and K. Fukui, *Int. J. Quantum Chem.*, 1996, **60**, 401-408.
91 O. Henri-Rousseau and F. Texier, *J. Chem. Educ.*, 1978, **55**, 437-441.
92 M. Sawada, M. Ichimura, Y. Yukawa, T. Nakachi and Y. Tsuno, *Bull. Chem. Soc. Jpn.*, 1980, **53**, 2055-2060.
93 B. Uno and T. Kubota, *J. Chem. Soc. Jpn.*, 1991, **2**, 101-109.
94 R. H. Page, Y. R. Shen and Y. T. Lee, *J. Chem. Phys.*, 1988, **88**, 5362-5376.
95 T. Ebata, N. Mizuochi, T. Watanabe and N. Mikami*, J. Phys. Chem.*, 1996, **100**, 546-550.
96 R. Matsumoto, K. Sakeda, Y. Matsushita, T. Suzuki and T. Ichimura, *J. Mol. Struct.*, 2005, **735-736**, 153-167.
97 N. Aizawa, Y. Harabuchi, S. Maeda, Y.-J. Pu, *Nature Commun.*, 2020, **11**, 3909.
98 T. Horio, Y. Suzuki and T. Suzuki, *J. Chem. Phys.*, 2016, **145**, 044307.
99 S. Mai and L. Gonzalez, *Angew. Chem. Int. Ed.*, 2020, **59**, 16832-16846

100 F. D. Lewis, R. S. Kalgutkar and J.-S. Yang, *J. Am. Chem. Soc.*, 1999, **121**, 12045-12053.
101 J. A. Stearns and T. S. Zwier, *J. Phys. Chem. A*, 2003, **107**, 10717-10724.
102 N. G. K. Wong, J. A. Berenbeim, M. Hawkridge, E. Matthewsa and C. E. H. Dessent, *Phys. Chem. Chem. Phys.*, 2019, **21**, 14311-14321.
103 J. A. Berenbeim, N. G. K. Wong, M. C. R. Cockett, G. Berden, J. Oomens, A. M. Rijs, and C. E. H. Dessent, *J. Phys. Chem. A,* 2020, **124**, 2919-2930.